Proceedings of the XII International Symposium on Dynamic Problems of Mechanics (DINAME 2007),
P.S.Varoto and M.A.Trindade (editors), ABCM, Ilhabela, SP, Brazil, February 26 - March 2, 2007

Dynamic Analysis of Spherical Caps under Moving Loads using Mindlin Elements

A. R. de Faria[1] **and D. C. D. Oguamanam**[2]

[1] Instituto Tecnológico de Aeronáutica, CTA - ITA - IEM, São José dos Campos, SP 12228-900, Brazil

[2] Ryerson University, Dept. of Mech., Aero., and Industrial Engineering, Toronto, Ontario, Canada M5B 2K3

Abstract: The finite element method (FEM) is used for the first time to investigate the vibration response of a spherical cap to either moving force and moving mass. Significant errors are observed when the element used to model the spherical cap is the Mindlin element and when the load is located at off-nodal positions. Since the load is moving, it would forcibly be at off-nodal positions at several instants of time. The solution proposed is to remesh the spherical cap domain at all instants of time in order to guarantee that the load is always exactly on a node. The forward time integration is done by the Newmark method accompanied by a perturbation scheme to account for the inherent nonlinearities due to the moving mass modeling. The perturbation scheme is shown to be more accurate when the moving mass is much smaller than the spherical cap mass, which is a realistic situation. The finite element code implemented is compared and validated against a commercial finite element code. Two scenarios are investigated: traversing load along the equator and moving load orbiting the apex. Simulations are carried out for both moving force and mass.

Keywords: moving load, spherical cap, finite element

NOMENCLATURE

$\mathbf{A}$ = membrane stiffness matrix
$\mathbf{A}_s$ = zero order shear stiffness matrix
$\mathbf{B}$ = membrane-bending coupling stiffness matrix
$\mathbf{B}_s$ = first order shear stiffness matrix
C_{bI} = transformation matrix
$\mathbf{C}_m$ = moving load global damping matrix
$\mathbf{C}_{me}$ = moving load element damping matrix
$\mathbf{D}$ = bending stiffness matrix
$\mathbf{D}_s$ = second order shear stiffness matrix
$\mathbf{e}_\theta$, $\mathbf{e}_\phi$, $\mathbf{e}_n$ = versors in the local coordinate system
E = Young modulus
f = dummy function of θ and ϕ
$\mathbf{f}$ = global load vector
$\mathbf{f}_e$ = element load vector
$\mathbf{f}_m$ = moving load global load vector
$\mathbf{f}_{me}$ = moving load element load vector
g = gravitational acceleration
h = spherical cap thickness
$\mathbf{K}$ = global stiffness matrix
$\mathbf{K}_e$ = element stiffness matrix
$\mathbf{K}_m$ = moving load global stiffness matrix
$\mathbf{K}_{me}$ = moving load element stiffness matrix
$\bar{\mathbf{K}}$ = effective global stiffness matrix
m = concentrated moving mass
$\mathbf{M}$ = global mass matrix
$\mathbf{M}_e$ = element mass matrix
$\mathbf{M}_m$ = moving load global mass matrix
$\mathbf{M}_{me}$ = moving load element mass matrix
$\mathbf{N}$ = vector of interpolation functions
$\mathbf{N}_u$ = vector of longitudinal displacement interpolation functions
$\mathbf{N}_v$ = vector of meridional displacement interpolation functions
$\mathbf{N}_w$ = vector of transverse displacements interpolation functions
$\mathbf{N}_{\psi_\theta}$ = vector of meridional rotation interpolation functions
$\mathbf{N}_{\psi_\phi}$ = vector of longitudinal rotation interpolation functions
$\mathbf{p}$ = position vector of the moving mass
$\mathbf{q}$ = global vector of nodal degrees of freedom
$\mathbf{q}_0$ = zero order perturbation displacements
$\mathbf{q}_1$ = first order perturbation displacements
$\mathbf{q}_2$ = second order perturbation displacements
$\mathbf{q}_e$ = element vector of nodal degrees of freedom
$\mathbf{q}_i$ = ith order perturbation displacements
$\mathbf{q}_u$ = element vector of longitudinal displacements
$\mathbf{q}_v$ = element vector of meridional displacements
$\mathbf{q}_w$ = element vector of transverse displacements
$\mathbf{q}_{\psi_\theta}$ = element vector of meridional rotations
$\mathbf{q}_{\psi_\phi}$ = element vector of longitudinal rotations
$\mathbf{Q}$ = in-plane matrix of material stiffness
$\mathbf{Q}_s$ = transverse shear matrix of material stiffness
R = spherical cap radius
$\mathbf{r}$ = position vector of a point in the cap
t = time
T = total kinetic energy
T_c = spherical cap kinetic energy
T_m = moving mass kinetic energy
u = longitudinal displacement
$u^* = u + h\psi_\theta/2$
$\bar{u}$ = mid point longitudinal displacement
U_c = spherical cap strain energy
U_m = gravitational potential energy
v = meridional displacement
$v^* = v + h\psi_\phi/2$
$\bar{v}$ = mid point meridional displacement
w, $\bar{w}$ = transverse displacement
X, Y, Z = Cartesian global coordinates
z = through the thickness coordinate

Greek Symbols

α = aperture angle
γ = out-of-plane shear strains
γ^0 = mid point out-of-plane shear strains
δ = variational operator
Δt = time step
ε = in-plane strains
ε^0 = mid point in-plane strains
θ = spherical coordinate
κ^i = mid point in-plane curvatures
κ^s = mid point out-of-plane shear curvatures
ν = Poisson ration
ρ = spherical cap mass density
ϕ = spherical coordinate
ψ_θ = meridional rotation
ψ_ϕ = longitudinal rotation
Ω = spherical cap domain

INTRODUCTION

Modeling of structures traversed by moving loads is often required in several ares such as ocean, aerospace and civil engineering. Examples of such structures are: airport runaways, railroads, bridges and overhead cranes (Stokes, 1849; Oguamanam, Hansen and Heppler, 1998; Pesterev and Bergman, 1997; Michaltsos, Sophianopoulos and Kounadis, 1996; Sadiku and Leipholz, 1987; Stanišić, 1985; Hino *et al.*, 1984; Olsson, 1985; Gbadeyan and Oni, 1995; Gbadeyan and Oni, 1992; Frýba, 1972). The majority of the works conducted on the subject relied on either beam (Stokes, 1849; Oguamanam, Hansen and Heppler, 1998; Pesterev and Bergman, 1997; Michaltsos, Sophianopoulos and Kounadis, 1996; Sadiku and Leipholz, 1987; Stanišić, 1985; Hino *et al.*, 1984) or plate (Gbadeyan and Oni, 1992, 1995) models. Few authors proposed more general techniques aimed at modeling of real world structures of arbitrary geometry traversed by moving loads (Olsson, 1985; Frýba, 1972). Even when they did, the authors limited themselves to showing traditional examples of beam or plate type of structures.

There is undoubtedly a lot of research about spherical caps although no attempt has ever been made to study the response of this type structure under moving loads. The term moving load is applied either to refer to a moving force or a moving mass. However, spherical structures are more and more employed, specially in marine and submarine applications (Souza and Croll, 1980) where they are subjected to traversing loads (Gbadeyan and Oni, 1992). Large oil reservoirs are a typical application of spherical caps that are routinely subjected to moving loads during maintenance.

This article presents a study of the dynamic behavior of a spherical cap subjected to a moving concentrated load. The finite element governing equations of motion are obtained through the energy functional and Lagrange bilinear elements (Hughes, 1987). Selective reduced integration is used to eliminate the possibility of shear locking. Static and free vibration analyses of the spherical cap are made with the finite element code implemented as well as the commercial code MSC.Nastran, in order to validate the code implemented.

The numerical method selected to integrate the equation of motion in time is the Newmark method. The inertial effects of the moving mass are taken into account through a perturbation technique that permits the use of the traditional Newmark method without modifications as opposed to the work of Olsson (1985) where a special procedure is employed. Essentially, the dynamic response is written as an infinite series of terms where each term is smaller than its preceding in some norm. In this context, it is observed that the moving force problem corresponds to the solution of the perturbed problem when only the first term in the series is retained. It is therefore possible to investigate what are the differences between the moving force and the moving mass models. This is an study important since Sadiku and Leipholz (1987), Pesterev and Bergman (1997), and by Gbadeyan and Oni (1995) have shown that the moving force model does not always provides upper bounds for the moving mass situation.

The accuracy of the results rapidly deteriorates when the concentrated load is at an off-nodal position, unless a prohibitive mesh refinement is used. It happens because of the finite element implemented that is based on Reissner assumptions (Reissner, 1941). The strategy to overcome this difficulty without using fine meshes is to remesh the domain whenever the concentrated load falls off a nodal position, thereby maintaining accuracy. Remeshing strategies have been used previously in structural dynamics problems (Dutta, 2002) in order to enhance accuracy.

Souza and Croll (1980) observed that, due to the spherical coordinates, the governing spherical cap equations possess a singularity at the apex. Two approached have been proposed to go about this problem. Souza and Croll (1980) placed a very small hole in the apex and verified that no significant error is incurred. Zarghamee and Robinson (1967) and Kraus (1967) intentionally modify the governing equations in the neighborhood of the apex to enforce continuity of the solution. The solution proposed in this paper is to recognize that the singularity stems from the spherical coordinates that possess singularities at the poles. Hence, the spherical cap domain is positioned away from the poles, in the equatorial region.

EQUATION OF MOTION

A spherical cap with a moving mass m is shown in Fig. 1. The mass m traverses the spherical cap top surface with known velocity and acceleration. The spherical cap radius is R and its aperture angle is α. The Cartesian inertial frame of reference XYZ has its origin in the center the sphere and is accompanied by the versors $\mathbf{e}_x$, $\mathbf{e}_y$, and $\mathbf{e}_z$, along the X, Y, and Z axes respectively. A moving reference system is associated with the moving mass and has versors $\mathbf{e}_\theta$ tangent to the meridian curve, $\mathbf{e}_\phi$ tangent to the longitudinal curve and $\mathbf{e}_n$ normal to the spherical surface.

Following Mindlin assumptions, the in-plane displacements $\bar{u}$ and $\bar{v}$ vary linearly along the shell thickness whereas transverse displacement $\bar{w}$ is constant along the shell thickness. Hence,

$$\begin{aligned} \bar{u}(\theta,\phi,z,t) &= u(\theta,\phi,t)+z\psi_\theta(\theta,\phi,t) \\ \bar{v}(\theta,\phi,z,t) &= v(\theta,\phi,t)+z\psi_\phi(\theta,\phi,t) \\ \bar{w}(\theta,\phi,z,t) &= w(\theta,\phi,t) \end{aligned} \tag{1}$$

The displacement fields in Eq. (1) are described in the moving frame of reference. The transformation matrix C_{bI} (from moving mass to XYZ frames) is given by:

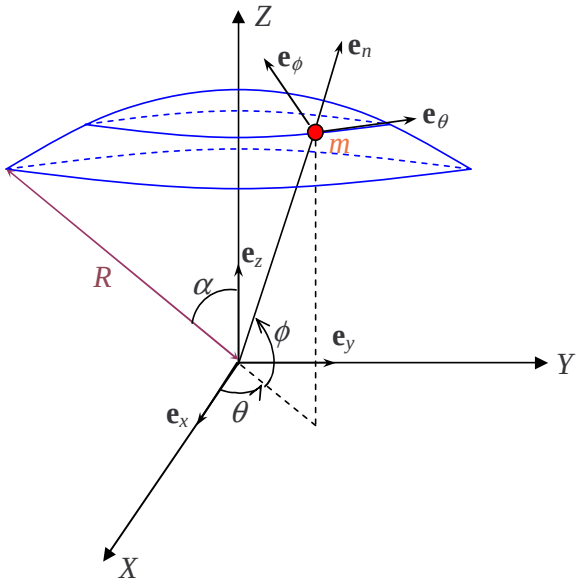

Figure 1 – Schematic of a spherical cap with moving load.

$$C_{bI} = \begin{bmatrix} -\sin\theta & -\sin\phi\cos\theta & \cos\phi\cos\theta \\ \cos\theta & -\sin\phi\sin\theta & \cos\phi\sin\theta \\ 0 & \cos\phi & \sin\phi \end{bmatrix} \tag{2}$$

Using Mindlin assumptions in Eq. (1) and the strain $\times$ displacement relations in Wang (1953), the linear strain $\times$ displacement relations applicable to the spherical cap can be written as

$$\varepsilon = \left\{ \begin{array}{c} \frac{1}{R\cos\phi}u_{,\theta} - \frac{\tan\phi}{R}v + \frac{1}{R}w \\ \frac{1}{R}v_{,\phi} + \frac{1}{R}w \\ \frac{1}{R}u_{,\phi} + \frac{\tan\phi}{R}u + \frac{1}{R\cos\phi}v_{,\theta} \end{array} \right\} + z \left\{ \begin{array}{c} \frac{1}{R\cos\phi}\psi_{\theta,\theta} - \frac{\tan\phi}{R}\psi_\phi \\ \frac{1}{R}\psi_{\phi,\phi} \\ \frac{1}{R}\psi_{\theta,\phi} + \frac{\tan\phi}{R}\psi_\theta + \frac{1}{R\cos\phi}\psi_{\phi,\theta} \end{array} \right\} = \varepsilon^0 + z\kappa^i$$

$$\gamma = \left\{ \begin{array}{c} \psi_\theta - \frac{1}{R}u + \frac{1}{R\cos\phi}w_{,\theta} \\ \psi_\phi - \frac{1}{R}v + \frac{1}{R}w_{,\phi} \end{array} \right\} + z \left\{ \begin{array}{c} -\frac{1}{R}\psi_\theta \\ -\frac{1}{R}\psi_\phi \end{array} \right\} = \gamma^0 + z\kappa^s \tag{3}$$

where ε^0 and γ^0 are the middle surface strains and κ^i and κ^s are the changes in curvatures.

The strain energy of the spherical cap can be written with the introduction of the in-plane matrix of material stiffness $\mathbf{Q}$ and the transverse shear matrix of material stiffness $\mathbf{Q}_s$ such that

$$U_c = \frac{1}{2}\int_\Omega \left\{ \begin{array}{c} \varepsilon^0 \\ \kappa^i \end{array} \right\}^T \begin{bmatrix} \mathbf{A} & \mathbf{B} \\ \mathbf{B} & \mathbf{D} \end{bmatrix} \left\{ \begin{array}{c} \varepsilon^0 \\ \kappa^i \end{array} \right\} d\Omega + \frac{1}{2}\int_\Omega \left\{ \begin{array}{c} \gamma^0 \\ \kappa^s \end{array} \right\}^T \begin{bmatrix} \mathbf{A}_s & \mathbf{B}_s \\ \mathbf{B}_s & \mathbf{D}_s \end{bmatrix} \left\{ \begin{array}{c} \gamma^0 \\ \kappa^s \end{array} \right\} d\Omega \tag{4}$$

where

$$(\mathbf{A},\mathbf{B},\mathbf{D}) = \int_{-h/2}^{h/2}(1,z,z^2)\mathbf{Q}dz \quad , \quad (\mathbf{A}_s,\mathbf{B}_s,\mathbf{D}_s) = \int_{-h/2}^{h/2}(1,z,z^2)\mathbf{Q}_s dz \quad ,$$

h is the spherical cap thickness and Ω is the spherical cap domain ($d\Omega = R^2\cos\phi\, d\theta d\phi$). Assuming that gravity is along the negative Z direction, the gravitational potential energy of the moving mass U_m is

$$U_m = mg\left[\left(v + \frac{h}{2}\psi_\phi\right)\cos\phi + w\sin\phi\right] \tag{5}$$

The position vector $\mathbf{r}$ of an arbitrary point in the spherical cap may be expressed as

$$\mathbf{r} = (u + z\psi_\theta)\,\mathbf{e}_\theta + (v + z\psi_\phi)\,\mathbf{e}_\phi + (R + w)\,\mathbf{e}_n \tag{6}$$

The position of the moving mass, $\mathbf{p}$, is written as

$$\mathbf{p} = \left(u + \frac{h}{2}\psi_\theta\right)\mathbf{e}_\theta + \left(v + \frac{h}{2}\psi_\phi\right)\mathbf{e}_\phi + (R+w)\,\mathbf{e}_n = u^*\mathbf{e}_\theta + v^*\mathbf{e}_\phi + (R+w)\,\mathbf{e}_n \tag{7}$$

The total kinetic energy of the system T is the summation of the spherical cap kinetic energy T_c and the moving mass kinetic energy T_m. T_c can be expressed as

$$T_c = \frac{1}{2}\int_V \rho\left[\left(\frac{\partial \bar{u}}{\partial t}\right)^2 + \left(\frac{\partial \bar{v}}{\partial t}\right)^2 + \left(\frac{\partial w}{\partial t}\right)^2\right] dV = \frac{1}{2}\int_\Omega \rho h\left[\dot{u}^2 + \dot{v}^2 + \dot{w}^2 + \frac{h^2}{12}\left(\dot{\psi}_\theta^2 + \dot{\psi}_\phi^2\right)\right] d\Omega \tag{8}$$

whereas T_m may be written as

$$T_m = \frac{m}{2}\frac{d\mathbf{p}}{dt}\cdot\frac{d\mathbf{p}}{dt} \tag{9}$$

In order to compute T_m in Eq. (9) the time derivatives of $\mathbf{p}$ must be evaluated. This must be done with the transformation matrix C_{bI} given in Eq. (2) since the versors $\mathbf{e}_\theta$, $\mathbf{e}_\phi$ and $\mathbf{e}_n$ are time dependant. Hence, time derivatives of $\mathbf{e}_\theta$, $\mathbf{e}_\phi$ and $\mathbf{e}_n$ must be obtained.

$$\frac{d\mathbf{e}_\theta}{dt} = \dot{\theta}\sin\phi\;\mathbf{e}_\phi - \dot{\theta}\cos\phi\;\mathbf{e}_n,\;\; \frac{d\mathbf{e}_\phi}{dt} = -\dot{\theta}\sin\phi\;\mathbf{e}_\theta - \dot{\phi}\;\mathbf{e}_n,\;\; \frac{d\mathbf{e}_n}{dt} = \dot{\theta}\cos\phi\;\mathbf{e}_\theta + \dot{\phi}\;\mathbf{e}_\phi \tag{10}$$

Differentiation of $\mathbf{p}$ in Eq. (7) with respect to time, consideration of Eq. (10) and substitution into Eq. (9) yields

$$\begin{aligned} T_m \;=\; & \frac{m}{2}\left\{\left(\frac{du^*}{dt}\right)^2 + \left(\frac{dv^*}{dt}\right)^2 + \left(\frac{dw}{dt}\right)^2 + 2\dot{\theta}\left[(R+w)\cos\phi - v^*\sin\phi\right]\frac{du^*}{dt} + \right. \\ & 2\left[u^*\dot{\theta}\sin\phi + \dot{\phi}(R+w)\right]\frac{dv^*}{dt} - 2\left[u^*\dot{\theta}\cos\phi + \dot{\phi}v^*\right]\frac{dw}{dt} + \\ & \left.\dot{\theta}^2\left[(R+w)\cos\phi - v^*\sin\phi\right]^2 + \left[u^*\dot{\theta}\sin\phi + (R+w)\dot{\phi}\right]^2 + \left[u^*\dot{\theta}\cos\phi + v^*\dot{\phi}\right]^2\right\} \end{aligned} \tag{11}$$

The first variation of T_m given in Eq. (11) is taken and, integration by parts after integration in time leads to:

$$\begin{aligned} \int_{t_1}^{t_2}\delta T_m dt \;=\; & \int_{t_1}^{t_2} m\left[-\frac{d^2u^*}{dt^2} + u^*\dot{\theta}^2 + 2v^*\dot{\theta}\dot{\phi}\cos\phi + 2\frac{dv^*}{dt}\dot{\theta}\sin\phi + 2(R+w)\dot{\theta}\dot{\phi}\sin\phi - \right. \\ & \left. -2\frac{dw}{dt}\dot{\theta}\cos\phi + v^*\ddot{\theta}\sin\phi - (R+w)\ddot{\theta}\cos\phi\right]\delta u^* dt + \\ & \int_{t_1}^{t_2} m\left[-\frac{d^2v^*}{dt^2} + v^*\dot{\phi}^2 + v^*\dot{\theta}^2\sin^2\phi - (R+w)\dot{\theta}^2\sin\phi\cos\phi - 2\frac{dw}{dt}\dot{\phi} - \right. \\ & \left. -2\frac{du^*}{dt}\dot{\theta}\sin\phi - u^*\ddot{\theta}\sin\phi - (R+w)\ddot{\phi}\right]\delta v^* dt + \\ & \int_{t_1}^{t_2} m\left[-\frac{d^2w}{dt^2} + (R+w)\dot{\theta}^2\cos^2\phi - v^*\dot{\theta}^2\sin\phi\cos\phi + 2\frac{du^*}{dt}\dot{\theta}\cos\phi + \right. \\ & \left. +(R+w)\dot{\phi}^2 + 2\frac{dv^*}{dt}\dot{\phi} + u^*\ddot{\theta}\cos\phi + v^*\ddot{\phi}\right]\delta w dt \end{aligned} \tag{12}$$

Total derivatives are present in Eqs. (9)-(12). However, convective term arise since the mass position may vary with time. Using the chain rule, first and second total derivatives are computed through Eq. (13):

$$\begin{aligned} \frac{df}{dt} \;&=\; \frac{\partial f}{\partial t} + \frac{\partial\theta}{\partial t}\frac{\partial f}{\partial\theta} + \frac{\partial\phi}{\partial t}\frac{\partial f}{\partial\phi} = \dot{f} + \dot{\theta}f_{,\theta} + \dot{\phi}f_{,\phi} \\ \frac{d^2f}{dt^2} \;&=\; \ddot{f} + 2\dot{\theta}\dot{f}_{,\theta} + 2\dot{\phi}\dot{f}_{,\phi} + \ddot{\theta}f_{,\theta} + \ddot{\phi}f_{,\phi} + \dot{\theta}^2 f_{,\theta\theta} + \dot{\phi}^2 f_{,\phi\phi} + 2\dot{\theta}\dot{\phi}f_{,\theta\phi} \end{aligned} \tag{13}$$

where f is a dummy function of θ and ϕ.

It was mentioned that the spherical coordinates possess singularities at the poles. According to Fig. 1, the computation of the strain $\times$ displacement relations would result in singularity due to division by zero when $\phi = \pm\pi/2$. This singularity might be avoided by introducing an artificial infinitesimal hole centered about the apex as implemented by Souza and Croll (1980) or the method adopted by Zarghamee and Robinson (1967) and by Kraus (1967) where the equations of motion are modified within a neighborhood of the apex while enforcing continuity conditions.

These strategies have been used in the past and provided satisfactory results. However, the traversing load is expected to cross the spherical cap and be, at some time, exactly at the apex, what precludes the first strategy. The second strategy involves special mathematical treatments that are inappropriate for dynamic problems. The spherical cap is only a portion of the whole sphere. Hence, theoretically, any cap that does not contain the poles would not suffer from the singularity effects. Hence, the approach adopted in this paper is to consider a spherical cap in the region of the equator. In particular, the spherical cap is aligned with the X axis and gravity is assumed to act in the negative X axis direction. This particular position of the domain does not alter the previously derived equations, except for the relatively simple Eq. (5). The new equation for the gravitational potential energy is

$$U_m = -mg\left[u^* \sin\theta + v^* \sin\phi\cos\theta - w\cos\phi\cos\theta\right] \tag{14}$$

NUMERICAL PROCEDURES

The finite element method requires discretization of the problem. The vector of shape functions is $\mathbf{N}$ and $\mathbf{q}_e$ is the element vector of nodal degrees of freedom $\mathbf{q}_e = \{\ \mathbf{q}_u^T \quad \mathbf{q}_v^T \quad \mathbf{q}_w^T \quad \mathbf{q}_{\psi_\theta}^T \quad \mathbf{q}_{\psi_\phi}^T\ \}^T$. Exact displacements and rotations are substituted by their finite element counterparts through the use of Eq. (15).

$$\begin{aligned}
u &= [\ \mathbf{N}\ \ \mathbf{0}\ \ \mathbf{0}\ \ \mathbf{0}\ \ \mathbf{0}\ ]\mathbf{q}_e \equiv \mathbf{N}_u\mathbf{q}_e & v &= [\ \mathbf{0}\ \ \mathbf{N}\ \ \mathbf{0}\ \ \mathbf{0}\ \ \mathbf{0}\ ]\mathbf{q}_e \equiv \mathbf{N}_v\mathbf{q}_e \\
w &= [\ \mathbf{0}\ \ \mathbf{0}\ \ \mathbf{N}\ \ \mathbf{0}\ \ \mathbf{0}\ ]\mathbf{q}_e \equiv \mathbf{N}_w\mathbf{q}_e & \psi_\theta &= [\ \mathbf{0}\ \ \mathbf{0}\ \ \mathbf{0}\ \ \mathbf{N}\ \ \mathbf{0}\ ]\mathbf{q}_e \equiv \mathbf{N}_{\psi_\theta}\mathbf{q}_e \\
\psi_\phi &= [\ \mathbf{0}\ \ \mathbf{0}\ \ \mathbf{0}\ \ \mathbf{0}\ \ \mathbf{N}\ ]\mathbf{q}_e \equiv \mathbf{N}_{\psi_\phi}\mathbf{q}_e & u^* &= [\ \mathbf{N}\ \ \mathbf{0}\ \ \mathbf{0}\ \ \tfrac{h}{2}\mathbf{N}\ \ \mathbf{0}\ ]\mathbf{q}_e \equiv \mathbf{N}_{u^*}\mathbf{q}_e \\
& & v^* &= [\ \mathbf{0}\ \ \mathbf{N}\ \ \mathbf{0}\ \ \mathbf{0}\ \ \tfrac{h}{2}\mathbf{N}\ ]\mathbf{q}_e \equiv \mathbf{N}_{v^*}\mathbf{q}_e
\end{aligned} \tag{15}$$

The usual element stiffness matrix $\mathbf{K}_e$, element mass matrix $\mathbf{M}_e$ and element load vector $\mathbf{f}_e$ can be obtained when the expressions for u, v, w, ψ_θ and ψ_ϕ given in Eq. (15) are substituted into Eqs. (4), (8) and (14). The moving load element stiffness matrix $\mathbf{K}_{me}$, moving load element mass matrix $\mathbf{M}_{me}$, moving load damping matrix $\mathbf{C}_{me}$ and moving load element load vector $\mathbf{f}_{me}$ can be obtained similarly by substitution of u, v, w, ψ_θ and ψ_ϕ into Eq. (12) and recalling Eq. (13). $\mathbf{K}_{me}$, $\mathbf{M}_{me}$, $\mathbf{C}_{me}$ and $\mathbf{f}_{me}$ are detailed in Appendix A. Traditional assembly of the element arrays yields the governing matrix equations:

$$(\mathbf{M}+\mathbf{M}_m)\ddot{\mathbf{q}} + \mathbf{C}_m\dot{\mathbf{q}} + (\mathbf{K}+\mathbf{K}_m)\mathbf{q} = \mathbf{f}+\mathbf{f}_m \tag{16}$$

Two types of arrays can be observed in Eq. (16): those that are independent of θ, ϕ, $\dot{\theta}$, $\dot{\phi}$, $\ddot{\theta}$ and $\ddot{\phi}$ ($\mathbf{K}$, $\mathbf{M}$, $\mathbf{M}_m$, $\mathbf{f}$) and those that depend on θ, ϕ and their time derivatives ($\mathbf{K}_m$, $\mathbf{C}_m$, $\mathbf{f}_m$).

The equations of motion, Eq. (16), reduce to that of a spherical cap with a static concentrated mass when the time derivatives of θ, ϕ are zero. The moving mass changes the stiffness of the system and adds a forcing term. However, its effects cannot be determined beforehand since they depend on the moving mass velocity and acceleration. As observed in Appendix A, $\mathbf{K}_m$, $\mathbf{C}_m$ are nonsymmetric matrices dependent on θ, ϕ and their time derivatives.

Since $\mathbf{K}_m$ and $\mathbf{C}_m$ vary with time and are nonsymmetric, a traditional forward integration scheme cannot be directly employed. This fact motivates the use of a perturbation approach to integrate the equations of motion in time. This approach consists in separating the nonlinear, nonsymmetric original problem into a number of linear, symmetric sub-problems by representing the total displacement as a series:

$$\mathbf{q} = \mathbf{q}_0 + \mathbf{q}_1 + \mathbf{q}_2 + \ldots + \mathbf{q}_n \tag{17}$$

and admitting that each term in the series is smaller than its preceding term in some norm. Substituting Eq. (17) into (16) and collecting terms in $\mathbf{q}_0$, $\mathbf{q}_1$,...,$\mathbf{q}_n$, yields the sub-problems:

$$\begin{aligned}
\mathbf{M}\ddot{\mathbf{q}}_0 + \mathbf{K}\mathbf{q}_0 &= \mathbf{f} \\
\mathbf{M}\ddot{\mathbf{q}}_1 + \mathbf{K}\mathbf{q}_1 &= \mathbf{f}_m - \mathbf{M}_m\ddot{\mathbf{q}}_0 - \mathbf{C}_m\dot{\mathbf{q}}_0 - \mathbf{K}_m\mathbf{q}_0 \\
\mathbf{M}\ddot{\mathbf{q}}_2 + \mathbf{K}\mathbf{q}_2 &= -\mathbf{M}_m\ddot{\mathbf{q}}_1 - \mathbf{C}_m\dot{\mathbf{q}}_1 - \mathbf{K}_m\mathbf{q}_1
\end{aligned}$$

$$\vdots$$
$$\mathbf{M}\ddot{\mathbf{q}}_n + \mathbf{K}\mathbf{q}_n = -\mathbf{M}_m\ddot{\mathbf{q}}_{n-1} - \mathbf{C}_m\dot{\mathbf{q}}_{n-1} - \mathbf{K}_m\mathbf{q}_{n-1} \tag{18}$$

The left hand side of all Eqs. (18) are of the form $\mathbf{M}\ddot{\mathbf{q}}_i + \mathbf{K}\mathbf{q}_i$. Since $\mathbf{K}$ and $\mathbf{M}$ are constant, symmetric matrices, a traditional time integration scheme such as the Newmark method can be used without modifications to solve numerically each of Eqs. (18) individually. The effective stiffness matrix of each of the sub-problems assume the same form: $\overline{\mathbf{K}}\mathbf{q}_{i+1} = \overline{\mathbf{f}}(\mathbf{q}_i, \theta, \phi, \dot{\theta}, \dot{\phi}, \ddot{\theta}, \ddot{\phi})$. Because of this, only one matrix decomposition of $\overline{\mathbf{K}}$ is required for all sub-problems. Subsequently, each sub-problem is solved sequentially from $i = 0$ to n.

Determination of the number of terms n to be used in the series depends on the relative inertia of the moving mass compared to the spherical cap. If the moving mass is much smaller than the structure mass, then fewer terms can be used. This claim has been rigorously proven by de Faria (2004). When the moving mass m is appreciable, a full nonlinear numerical procedure may be more adequate.

THE FINITE ELEMENT MODEL AND ADAPTIVE MESHES

The finite element code implemented is validated through comparison against the commercial code MSC.Nastran. A spherical cap fully clamped along its edge is used. Its geometric and material properties are shown in Table 1.

Table 1 – Material properties

Parameter	Value
ρ	7.8×10^3 kgm^{-3}
h	30.0 mm
E	2.08×10^{11} Nm^{-2}
ν	0.30
R	100.0 m
α	10^o

The finite element code used bilinear elements with four nodes and selective reduced integration to alleviate eventual shear locking. A static problem is initially solved where a concentrated force of 1,000 N is applied perpendicular to the cap at its apex and the transverse displacement under the force is computed. A free vibration simulation is also made to extract the five lowest natural frequencies. Results of the validation analyses are shown in Table 2 and compared against those found by MSC.Nastran. The mesh used in the present code has 768 elements whereas MSC.Nastran has 3,200 elements, i.e., MSC.Nastran used approximately four times more nodes. The results in Table 2 are accurate and reliable.

Table 2 – Verification of finite element code

Frequencies (Hz)			Apex deflection (mm)	
Mode	Present code	Nastran	Present code	Nastran
1	8.24	8.24		
2	8.30	8.31		
3	8.30	8.31	0.230	0.228
4	8.38	8.38		
5	8.38	8.38		

A simple numerical example suffices to understand why adaptive meshes are necessary in the present study. Take the spherical cap presented in Table 1 traversed quasi-statically by a moving force always parallel to the X axis. The point of application of the force is given by $R\cos\theta\ \mathbf{e}_x + R\sin\theta\ \mathbf{e}_y$, with $-\alpha \leq \theta \leq \alpha$. Figure 2 shows the concentrated force applied to eleven different points. Notice that the cap apex is positioned on the equator of the sphere in order to avoid singularities.

Fifty one static problems are solved applying 1,000 N concentrated forces along 51 equally spaced points along the curve $R\cos\theta\ \mathbf{e}_x + R\sin\theta\ \mathbf{e}_y$ with $-\alpha \leq \theta \leq \alpha$. The transverse displacements w under the applied force are presented in Fig. 3. These results are normalized with respect to the value of w obtained in Table 2. The results for the 40×80 MSC.Nastran fixed mesh and the 768 element adaptive mesh used by the present code are compared in Fig. 3.

It is obvious that the ripples seen in the MSc.Nastran results are numerically induced. They exist because the concentrated force is sometimes applied at off-nodal positions. On the other hand, the adaptive mesh makes sure that the force is applied always at a node. The correct results are found by MSC.Nastran when, by chance, the force is exactly at a node.

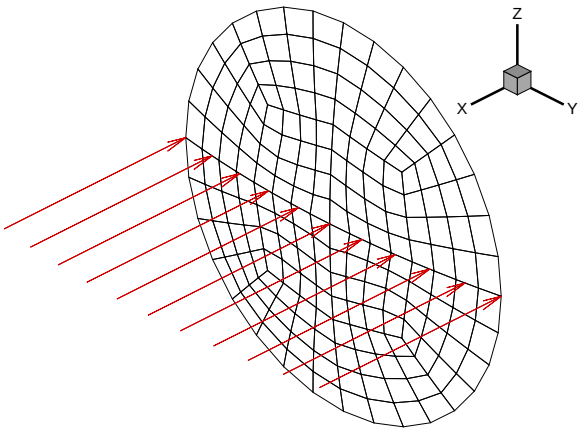

Figure 2 – Schematic of a repositioned spherical cap with moving force.

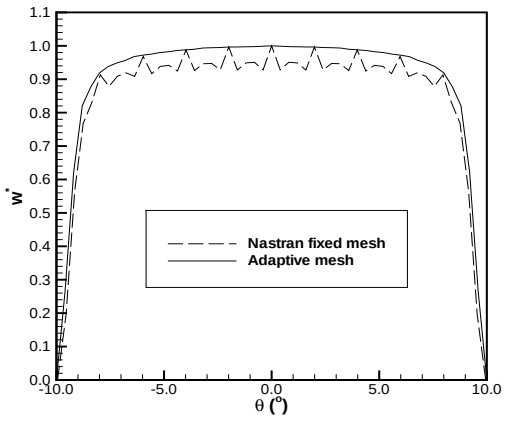

Figure 3 – Spherical cap and moving forces.

The difficulty with remeshing schemes is that the finite element matrices change once the mesh is changed. Moreover, numerical procedures to integrate the equations of motion in time are based on time steps where the current displacement, velocity and acceleration depends on information of the previous time step. Since the mesh in the previous time step was different, some kind of mapping of the old mesh onto the new mesh must be implemented.

The mapping strategy adopted can be understood in Fig. 4. Consider that the displacements (u, v, w) and rotations (ψ_x, ψ_y) at node i_{new} must be somehow obtained. The basic information required is to know which element in the old mesh contains node i_{new}. This allows one to find the local coordinates ξ, η of node i_{new}. Once the local coordinates are available, regular interpolation of the degrees of freedom of nodes i_{old}, j_{old}, k_{old} and l_{old} is used to compute the corresponding degrees of freedom at nodes i_{new}.

DYNAMIC SIMULATION AND DISCUSSION

Two situations are simulated: the moving force and the moving mass problems. In the moving force problem a concentrated force is assumed to move across the spherical cap surface but the moving mass m is zero. In this case matrices $\mathbf{K}_m$, $\mathbf{C}_m$, $\mathbf{M}_m$ and vector $\mathbf{f}_m$ are taken as zero since they are proportional to m (see appendix A). This observation considerably simplifies the numerics involved since just $\mathbf{q}_0 \neq \mathbf{0}$ whereas $\mathbf{q}_1 = \mathbf{q}_2 = ... = \mathbf{q}_n = \mathbf{0}$. When $m > 0$, the higher order terms $\mathbf{q}_1$, $\mathbf{q}_2$, ... , $\mathbf{q}_n$ are nonzero but increasingly small, i.e., $\mathbf{q}_1 << \mathbf{q}_2 << ... << \mathbf{q}_n$ In the simulations conducted in this work only four terms were enough to achieve good accuracy: $\mathbf{q}_0$, $\mathbf{q}_1$, $\mathbf{q}_2$, $\mathbf{q}_3$.

In the first scenario the moving load travels with constant velocity $\dot{\theta} = 0.01$ rd/s along the equator, departing from the edge and reaching the apex where it suddenly stops. Cap geometry is described in Table 1. The force is of 1,000 N and it is oriented parallel to the X axis. The moving mass is 101.93 kg since $g = 9.81\ m/s^2$. The fixed time step adopted is $\Delta t = 0.005$ s what can represent the contribution frequencies up to 20 Hz. The load reaches the apex in about 17.45 s but

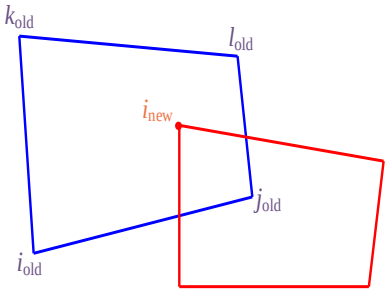

Figure 4 – Mesh mapping.

the simulation goes as far as 20 s. Advantage is taken of the symmetry about plane $Z = 0$ in order to model only half cap.

The simulation results are presented in in Figs. 5a-b. The curves seen in Figs. 5a-b are not too different from that of Fig. 3 for $-10^o \leq \theta \leq 0^o$. Therefore, it is clear that the dynamic effects are negligible when compared to the quasi-static simulation under concentrated force. After reaching the apex the mass stops and the spherical cap displays residual vibrations that, in real situations, eventually die out due to structural damping. What can be inferred is that the frequency content of the residual vibrations is high, i.e., modes associated with higher frequencies contribute to that kind of residual vibration.

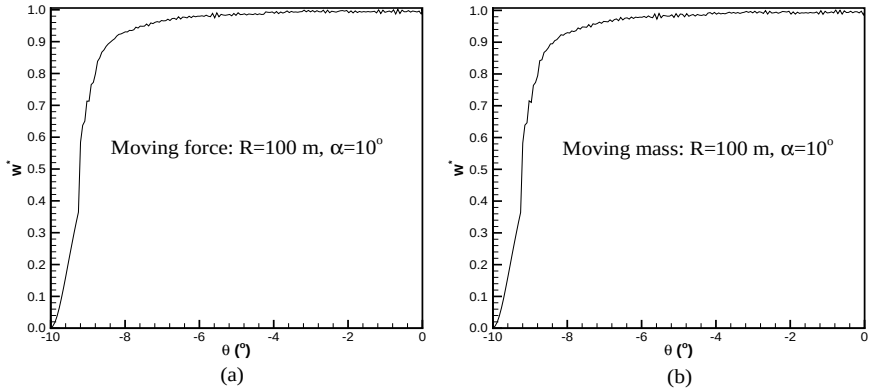

Figure 5 – Traversing loads moving on the equator.

The relative contribution of the terms $\mathbf{q}_0$, $\mathbf{q}_1$, $\mathbf{q}_2$ and $\mathbf{q}_3$ in the perturbation series, Eq. (17), can be seen in Fig. 6. The zero order term gives a far greater contribution than the other terms. Actually, it is observed that that magnitudes of $\mathbf{q}_1$, $\mathbf{q}_2$ and $\mathbf{q}_3$ are approximately 100, 1,000 and 10,000 times smaller than that of $\mathbf{q}_0$. This shows that the inertial effects of the moving mass are small in this particular problem.

In the second situation the load revolver around the apex along the curve $Y = r\cos\omega t$, $Z = r\sin\omega t$ with $r = 7$ m and $\omega = \pi/10$ rd/s, completing one revolution in 20 s. θ, ϕ and their time derivatives can be computed from the relations $Y = R\cos\phi\sin\theta$, $Z = R\sin\phi$ derived from Eq. (2). The spherical cap is initially deformed under the concentrated force the time step adopted is $\Delta t = 0.005$ s and the simulation lasts for 20 s.

The moving mass and moving force results are shown in in Figs. 7a-b. Notice that in Fig. 7a the normalized transverse displacement oscillates about $w^* = 0.925$, corresponding to the solution of the static problem $\mathbf{Kq} = \mathbf{f}$ obtained from Eq. (16). However, the normalized transverse displacement of the moving mass problem is about $w^* = 0.920$ as observed in Fig. 7b. These differences are a consequence of the moving mass inertial effects incorporated in matrix $\mathbf{K}_m$ and vector $\mathbf{f}_m$.

The effect of the spherical cap curvature in the dynamic behavior is investigated by keeping a constant value of $R\alpha$ and varying the radius R. Two configurations are considered: $R = 500$ m and $\alpha = 2^o$, and $R = 1,000$ m and $\alpha = 1^o$. The normalized apex transverse displacement for the moving force and moving mass orbiting the apex are presented in Figs. 8a-b and Figs. 9a-b. The apex transverse displacements of 1.068 mm ($R = 500$ m) and 2.004 mm ($R = 1,000$ m) were taken as normalization factors obtained when a transverse concentrated force of 1,000 N is applied at the apex.

The frequency content can be seen to increase as the curvature increases. This can be observed by comparison of Figs. 7, 8 and 9. Another interesting observation: differences between moving force and moving mass models tend to increase

with the curvature.

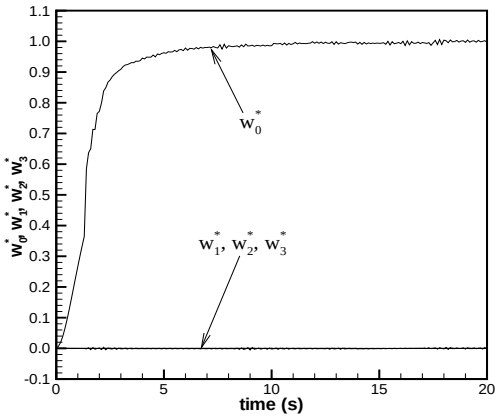

Figure 6 – Individual contribution of perturbation series terms.

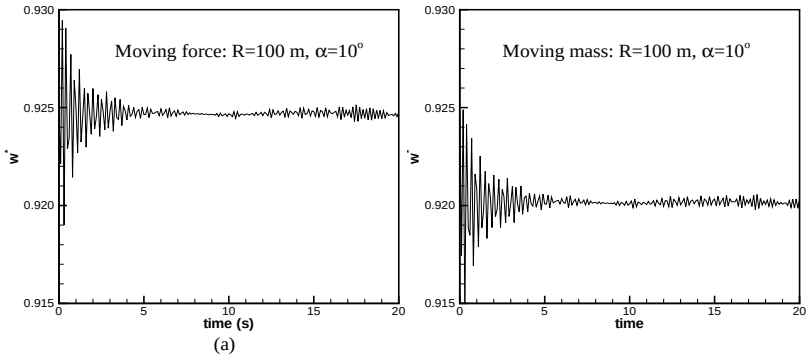

Figure 7 – Traversing loads orbiting the apex: $R = 100$ **m,** $\alpha = 10^o$**.**

CONCLUSIONS

A technique is presented to handle the problem of moving concentrated loads (mass or force) when relatively coarse finite element meshes are employed. The coarse mesh is adaptively modified in order to guarantee that the moving load is always exactly on a nodal position. Remeshing requires recomputation and decomposition of the global matrices involved. However, this computations should not be intense since it is assumed that coarse meshes are used.

The problem of loss of accuracy when the load is at a off-nodal position is inherent to the Mindlin element used. Elements whose interpolation functions are based on cubic polynomials do not suffer from this weakness but their numerical implements is far more intricate that the Mindlin element. Since the Mindlin type of element is the most commonly used in commercial finite element codes it is important to proposed alternative formulations such as the adaptive mesh scheme combined with a perturbation approach presented in this work. The formulation proposed was shown to work well in two scenarios and for either moving force or moving mass.

The perturbation technique adopted is able to separate the effects of a moving concentrated force from those of a moving concentrated mass. It shows that the inertial effects of the moving mass can be added to the moving force solution through solution of a series of linear sub-problems. Moreover, the number of sub-problems to be solved is small as long as the relative inertia between concentrated mass and base structure is small. When heavy masses move on lightweight structures more terms in the series are required or a more powerful nonlinear solver should be used.

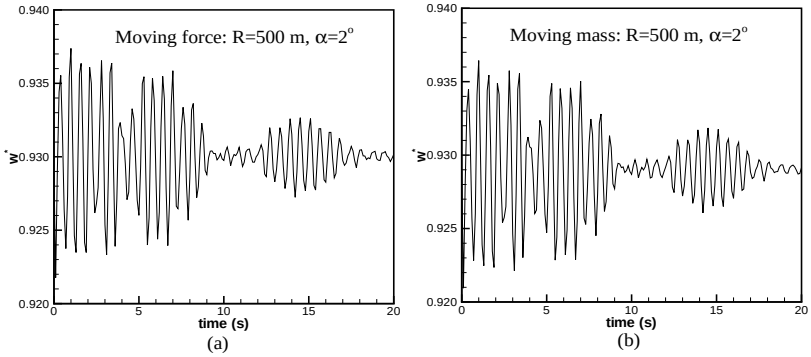

Figure 8 – Traversing loads orbiting the apex: $R = 500$ **m,** $\alpha = 2^o$**.**

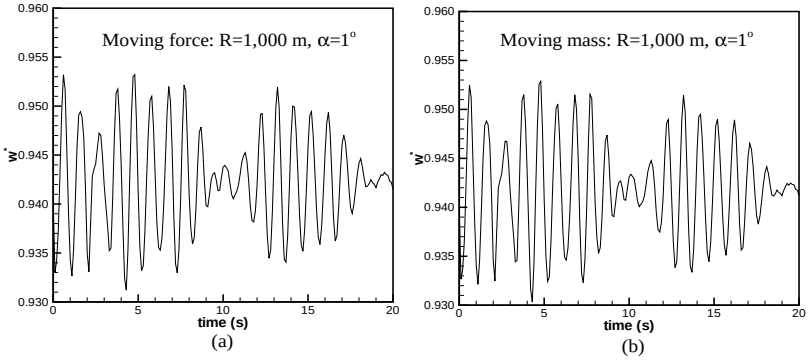

Figure 9 – Traversing loads orbiting the apex: $R = 1,000$ **m,** $\alpha = 1^o$**.**

REFERENCES

Dutta, A., 2002, "Adaptive finite element analysis of structures subjected to transient dynamic loads using time marching scheme", Computers & Structures, Vol. 80, pp. 2313-2319.

de Faria, A.R., 2004, "Finite element analysis of the dynamic response of cylindrical panels under traversing loads", European Journal of Mechanics A/Solids, Vol. 23, pp. 677-687.

Frýba, L., 1972, "Vibrations of Solids and Structures under Moving Load", Groningen: Noordhoff.

Gbadeyan, J.A. and Oni, S.T., 1995, "Dynamic behaviour of beams and rectangular plates under moving loads", Journal of Sound and Vibration, Vol. 182, pp. 677-695.

Gbadeyan, J.A. and Oni, S.T., 1992, "Dynamic response to moving concentrated masses of elastic plates on a non-Winkler elastic foundation", Journal of Sound and Vibration, Vol. 154, pp. 343-358.

Hino, J., Yoshimura, T., Konishi, K. and Ananthanarayana, N., 1984, "A finite element method prediction of the vibration of a bridge subjected to a moving vehicle load", Journal of Sound and Vibration, Vol. 96, pp. 45-53.

Hughes, T.J.R., 1987, "The Finite Element Method", New Jersey: Prentice-Hall, Inc.

Kraus, H., 1967, "Thin Elastic Shells", New York: John Wiley and Sons, Inc.

Michaltsos, G., Sophianopoulos, D. and Kounadis N., 1996, "The effect of a moving mass and other parameters on the dynamic response of a simple supported beam", Journal of Sound and Vibration, Vol. 191, pp. 357-362.

MSC.Nastran for windows. The MacNeal-Schwendler Corporation, California, U.S.A.

Oguamanam, D.C.D., Hansen, J. S. and Heppler, G.R., 1998, "Dynamic Response of an Overhead Crane System", Journal of Sound and Vibration, Vol. 213, pp. 889-906.

Olsson, M., 1985, "Finite element, modal co-ordinate analysis of structures subjected to moving loads", Journal of Sound and Vibration, Vol. 99, pp. 1-12.

Pesterev, A.V. and Bergman, L.A., 1997, "Response of elastic continuum carrying moving linear oscillator", ASCE Journal of Engineering Mechanics, Vol. 123, pp. 878-884.

Reissner, E., 1941, "A new derivation of the equations for the deformation of elastic shells", American Journal of Mathematics, Vol. 63, pp. 177-184.

Sadiku, S. and Leipholz, H.H.E., 1987, "On the dynamics of elastic systems with moving concentrated masses", Ingenieur-Archiv, Vol. 57, pp. 223-242.

de Souza, V.C.M. and Croll, J.G.A., 1980, "An energy analysis of the free vibrations of isotropic spherical shells", Journal of Sound and Vibration, Vol. 73, pp. 379-404.

Stanišić, M.M., 1985, "On a new theory of the dynamic behaviour of the structures carrying moving masses", Ingenieur-Archiv, Vol. 55, pp. 176-185.

Stokes, G.G., 1849, "Discussion of a differential equation relating to the breaking of railway bridges", Transactions of the Cambridge Philosophical Society, Vol. 5, pp. 707-735.

Wang, C.T., 1953, "Applied Elasticity", New York: McGraw-Hill Book Company, Inc.

Zarghamee, M.S. and Robinson, A.R., 1967, "A numerical method for analysis of free vibration of spherical shells", AIAA Journal, Vol. 5, pp. 1256-1261.

RESPONSIBILITY NOTICE

The authors are the only responsible for the printed material included in this paper.

APPENDIX A

$$\mathbf{M}_e = \int_\theta \int_\phi \rho h \begin{bmatrix} \mathbf{N}^T\mathbf{N} & \mathbf{0} & \mathbf{0} & \mathbf{0} & \mathbf{0} \\ \mathbf{0} & \mathbf{N}^T\mathbf{N} & \mathbf{0} & \mathbf{0} & \mathbf{0} \\ \mathbf{0} & \mathbf{0} & \mathbf{N}^T\mathbf{N} & \mathbf{0} & \mathbf{0} \\ \mathbf{0} & \mathbf{0} & \mathbf{0} & \frac{h^2}{12}\mathbf{N}^T\mathbf{N} & \mathbf{0} \\ \mathbf{0} & \mathbf{0} & \mathbf{0} & \mathbf{0} & \frac{h^2}{12}\mathbf{N}^T\mathbf{N} \end{bmatrix} R^2\cos\phi\, d\theta d\phi \tag{A.1}$$

$$\mathscr{B} = \begin{bmatrix} \frac{1}{R\cos\phi}\mathbf{N}_{,\theta} & -\frac{\tan\phi}{R}\mathbf{N} & \frac{1}{R}\mathbf{N} & \mathbf{0} & \mathbf{0} \\ \mathbf{0} & \frac{1}{R}\mathbf{N}_{,\phi} & \frac{1}{R}\mathbf{N} & \mathbf{0} & \mathbf{0} \\ \left(\frac{1}{R}\mathbf{N}_{,\phi} + \frac{\tan\phi}{R}\mathbf{N}\right) & \frac{1}{R\cos\phi}\mathbf{N}_{,\theta} & \mathbf{0} & \mathbf{0} & \mathbf{0} \\ \mathbf{0} & \mathbf{0} & \mathbf{0} & \frac{1}{R\cos\phi}\mathbf{N}_{,\theta} & -\frac{\tan\phi}{R}\mathbf{N} \\ \mathbf{0} & \mathbf{0} & \mathbf{0} & \mathbf{0} & \frac{1}{R}\mathbf{N}_{,\phi} \\ \mathbf{0} & \mathbf{0} & \mathbf{0} & \left(\frac{1}{R}\mathbf{N}_{,\phi} + \frac{\tan\phi}{R}\mathbf{N}\right) & \frac{1}{R\cos\phi}\mathbf{N}_{,\theta} \end{bmatrix} \tag{A.2}$$

$$\mathscr{B}_s = \begin{bmatrix} -\frac{1}{R}\mathbf{N} & \mathbf{0} & \frac{1}{R\cos\phi}\mathbf{N}_{,\theta} & \mathbf{N} & \mathbf{0} \\ \mathbf{0} & -\frac{1}{R}\mathbf{N} & \frac{1}{R}\mathbf{N}_{,\phi} & \mathbf{0} & \mathbf{N} \\ \mathbf{0} & \mathbf{0} & \mathbf{0} & -\frac{1}{R}\mathbf{N} & \mathbf{0} \\ \mathbf{0} & \mathbf{0} & \mathbf{0} & \mathbf{0} & -\frac{1}{R}\mathbf{N} \end{bmatrix} \tag{A.3}$$

$$\mathbf{K}_e = \int_\theta \int_\phi \left(\mathscr{B}^T \begin{bmatrix} \mathbf{A} & \mathbf{B} \\ \mathbf{B} & \mathbf{D} \end{bmatrix} \mathscr{B} + \mathscr{B}_s^T \begin{bmatrix} \mathbf{A}_s & \mathbf{B}_s \\ \mathbf{B}_s & \mathbf{D}_s \end{bmatrix} \mathscr{B}_s \right) R^2\cos\phi\, d\theta d\phi \tag{A.4}$$

$$\mathbf{f}_e = \int_\theta \int_\phi \rho h \begin{bmatrix} \sin\theta\, \mathbf{N}^T \\ \sin\phi\cos\theta\, \mathbf{N}^T \\ -\cos\phi\cos\theta\, \mathbf{N}^T \\ \frac{h}{2}\sin\theta\, \mathbf{N}^T \\ \frac{h}{2}\sin\phi\cos\theta\, \mathbf{N}^T \end{bmatrix} R^2\cos\phi\, d\theta d\phi \tag{A.5}$$

$$\mathbf{M}_{me} = m\left(\mathbf{N}_{u^*}^T\mathbf{N}_{u^*} + \mathbf{N}_{v^*}^T\mathbf{N}_{v^*} + \mathbf{N}_w^T\mathbf{N}_w\right) \tag{A.6}$$

$$\begin{aligned} \mathbf{C}_{me} = {} & 2m\mathbf{N}_{u^*}^T\left(\dot\theta\, \mathbf{N}_{u^*,\theta} + \dot\phi\, \mathbf{N}_{u^*,\phi} - \dot\theta\sin\phi\, \mathbf{N}_{v^*} + \dot\theta\cos\phi\, \mathbf{N}_w\right) \\ & 2m\mathbf{N}_{v^*}^T\left(\dot\theta\, \mathbf{N}_{v^*,\theta} + \dot\phi\, \mathbf{N}_{v^*,\phi} + \dot\phi\, \mathbf{N}_w + \dot\theta\sin\phi\, \mathbf{N}_{u^*}\right) \\ & 2m\mathbf{N}_w^T\left(\dot\theta\, \mathbf{N}_{w,\theta} + \dot\phi\, \mathbf{N}_{w,\phi} - \dot\theta\cos\phi\, \mathbf{N}_{u^*} - \dot\phi\, \mathbf{N}_{v^*}\right) \end{aligned} \tag{A.7}$$

$$\begin{aligned} \mathbf{K}_{me} = {} & m\,\mathbf{N}_{u^*}^T\left(\ddot\theta\, \mathbf{N}_{u^*,\theta} + \ddot\phi\, \mathbf{N}_{u^*,\phi} + \dot\theta^2\, \mathbf{N}_{u^*,\theta\theta} + \dot\phi^2\, \mathbf{N}_{u^*,\phi\phi} + 2\dot\theta\dot\phi\, \mathbf{N}_{u^*,\theta\phi} - \right. \\ & \dot\theta^2\, \mathbf{N}_{u^*} - 2\dot\theta\dot\phi\cos\phi\, \mathbf{N}_{v^*} - 2\dot\theta^2\sin\phi\, \mathbf{N}_{v^*,\theta} - 2\dot\theta\dot\phi\sin\phi\, \mathbf{N}_{v^*,\phi} - 2\dot\theta\dot\phi\sin\phi\, \mathbf{N}_w + \\ & \left. 2\dot\theta^2\cos\phi\, \mathbf{N}_{w,\theta} + 2\dot\theta\dot\phi\cos\phi\, \mathbf{N}_{w,\phi} - \ddot\theta\sin\phi\, \mathbf{N}_{v^*} + \ddot\theta\cos\phi\, \mathbf{N}_w\right) + \end{aligned}$$

$$
\begin{aligned}
& m\,\mathbf{N}_{v^*}^T\left(\ddot{\theta}\,\mathbf{N}_{v^*,\theta}+\ddot{\phi}\,\mathbf{N}_{v^*,\phi}+\dot{\theta}^2\,\mathbf{N}_{v^*,\theta\theta}+\dot{\phi}^2\,\mathbf{N}_{v^*,\phi\phi}+2\dot{\theta}\dot{\phi}\,\mathbf{N}_{v^*,\theta\phi}-\right.\\
& \dot{\phi}^2\,\mathbf{N}_{v^*}-\dot{\theta}^2\sin^2\phi\,\mathbf{N}_{v^*}+\dot{\theta}^2\sin\phi\cos\phi\,\mathbf{N}_w+2\dot{\theta}\dot{\phi}\,\mathbf{N}_{w,\theta}+2\dot{\phi}^2\,\mathbf{N}_{w,\phi}+\\
& \left.2\dot{\theta}^2\sin\phi\,\mathbf{N}_{u^*,\theta}+2\dot{\theta}\dot{\phi}\sin\phi\,\mathbf{N}_{u^*,\phi}+\ddot{\theta}\sin\phi\,\mathbf{N}_{u^*}+\ddot{\phi}\,\mathbf{N}_w\right)+\\
& m\,\mathbf{N}_w^T\left(\ddot{\theta}\,\mathbf{N}_{w,\theta}+\ddot{\phi}\,\mathbf{N}_{w,\phi}+\dot{\theta}^2\,\mathbf{N}_{w,\theta\theta}+\dot{\phi}^2\,\mathbf{N}_{w,\phi\phi}+2\dot{\theta}\dot{\phi}\,\mathbf{N}_{w,\theta\phi}-\right.\\
& \dot{\theta}^2\cos^2\phi\,\mathbf{N}_w+\dot{\theta}^2\sin\phi\cos\phi\,\mathbf{N}_{v^*}-2\dot{\theta}^2\cos\phi\,\mathbf{N}_{u^*,\theta}-2\dot{\theta}\dot{\phi}\cos\phi\,\mathbf{N}_{u^*,\phi}-\dot{\phi}^2\,\mathbf{N}_w-\\
& \left.2\dot{\theta}\dot{\phi}\,\mathbf{N}_{v^*,\theta}-2\dot{\phi}^2\,\mathbf{N}_{v^*,\phi}-\ddot{\theta}\cos\phi\,\mathbf{N}_{u^*}-\ddot{\phi}\,\mathbf{N}_{v^*}\right) \qquad \text{(A.8)}
\end{aligned}
$$

$$
\begin{aligned}
\mathbf{f}_{me} \;=\; & mR\left(2\dot{\theta}\dot{\phi}\sin\phi\mathbf{N}_{u^*}^T-\ddot{\theta}\cos\phi\,\mathbf{N}_{u^*}^T-\dot{\theta}^2\sin\phi\cos\phi\,\mathbf{N}_{v^*}^T-\ddot{\phi}\,\mathbf{N}_{v^*}^T+\right.\\
& \left.\dot{\theta}^2\cos^2\phi\,\mathbf{N}_w^T+\dot{\phi}^2\,\mathbf{N}_w^T\right) \qquad \text{(A.9)}
\end{aligned}
$$